Scientific Research Publishing

Engineering, 2018, 10, 730-758
http://www.scirp.org/journal/eng
ISSN Online: 1947-394X
ISSN Print: 1947-3931

Effect of Single Pass Laser Surface Treatment on Microstructure Evolution of Inoculated $Zr_{47.5}Cu_{45.5}Al_5Co_2$ and Non-Inoculated $Zr_{65}Cu_{15}Al_{10}Ni_{10}$ Bulk Metallic Glass Matrix Composites

Muhammad Musaddique Ali Rafique

Eastern Engineering Solutions LLC, Detroit, MI, USA
Email: ali.rafique@hotmail.com

How to cite this paper: Rafique, M.M.A. (2018) Effect of Single Pass Laser Surface Treatment on Microstructure Evolution of Inoculated $Zr_{47.5}Cu_{45.5}Al_5Co_2$ and Non-Inoculated $Zr_{65}Cu_{15}Al_{10}Ni_{10}$ Bulk Metallic Glass Matrix Composites. *Engineering*, **10**, 730-758.
https://doi.org/10.4236/eng.2018.1010052

Received: August 1, 2018
Accepted: October 23, 2018
Published: October 26, 2018

Abstract

Bulk metallic glass matrix composites are advocated to be material of future owing to their superior strength, hardness and elastic strain limit. However, they possess poor toughness which makes them unusable in any structural engineering application. Inoculation has been used as effective mean to overcome this problem. $Zr_{47.5}Cu_{45.5}Al_5Co_2$ bulk metallic glass matrix composites (BMGMC) inoculated with ZrC have shown considerable refinement in microstructure owing to heterogeneous nucleation. Efforts have also been made to exploit modern laser-based metal additive manufacturing to fabricate BMGMC parts in one step. However, the effect of laser on inoculated material is unknown. In this study, an effort has been made to apply single pass laser surface treatment on untreated and inoculated BMGMC samples. It is observed that laser treatment not only refine the microstructure but result in change of size, morphology and dispersion of CuZr B2 phase in base metal, heat affected zone and fusion zone in $Zr_{47.5}Cu_{45.5}Al_5Co_2$. A similar effect is observed for β-Zr and Zr_2Cu in non-inoculated $Zr_{65}Cu_{15}Al_{10}Ni_{10}$. This effect is documented with back scatter electron imaging.

Keywords

Additive, Bulk Metallic Glass, Composites, Inoculation, Phase

1. Introduction

Over time, there has always been a quest for hard, strong and tough material [1] [2] which can effectively withstand the loads encountered in practical extreme engineering problems. Various efforts have been made to achieve this [3] [4] and many new materials were developed over time. Although they were discovered in 1950s [5], very recently, bulk metallic glasses [6] [7] [8] [9] [10] have emerged as potential candidates to solve this problem [11]. They possess high hardness [12] [13] and strength due to parent glassy structure but have poor ductility, hence poor toughness and exhibit catastrophic failure under the action of external load [14] [15] [16]. This problem limits their application.

Effort has been made to overcome this problem by introducing crystallinity in the glassy matrix. This may be achieved by various means including; external [17] [18] [19] introduction of reinforcing particles (*ex situ*) or internal (*in-situ*) [20]-[26] precipitating of same during processing (solidification [27] [28] [29], devitrification [30] [31] [32] [33], powder metallurgy [34], foaming [35] or solid-state processing). However, this quest is still far from exhausted. *In-situ* introduction of precipitates during solidification have proved out to be best mechanism to tackle this problem and newer methods have been introduced to achieve this mostly by control of melt composition [36], chemistry, and adjustment of processing conditions [37] [38]. Successful introduction of precipitates to form composite structures was reported for the first time by Prof. Johnson's group at Caltech in 2000 [39]. Since then many groups in the world have produced a multitude of composites using similar philosophy [21] [28] [40]-[56].

Additive manufacturing has also emerged as new innovative and competitive route for a quick, efficient and one step solution to produce near net shape complex parts [57] [58] [59] [60] [61]. Components from nearly all types of metals and alloys can be produced by this technique (laser [58] [59] [60] [62] [63] or electron beam [64] [65] based) as the temperature obtained is a function of laser power and can be flexibly controlled over a wide range. Need and interest has also sparked in the use of this technique for microstructure control [54] [66] [67] [68], manipulation [69] [70] and manufacturing of parts by bulk metallic glasses and their composites [55] [67] [71] [72] [73]. Both simulation [55] [63] [65] [74]-[80] and experimental [64] [67] [68] [81] [82] methodologies have been rigorously applied to study, determine and ascertain the effect of various material and process parameters on final part quality and its properties. Different AM variants such as laser surface remelting [38] [54] [66] [67] [68] [69] [83]-[89], 3D printing [90] [91] [92] [93] LENS [94], welding [95] [96] [97], pulsing [98] [99], shock peening [100], and laser solid forming [66] [69] [98] [99] [100] [101] [102] have been successfully applied to fabricate parts of various types, size, nature and geometries.

Recently, an established grain refinement technique—inoculation [3] [103] [104] has been applied to Zr based bulk metallic glass matrix composites and found to successfully improve properties of as cast composites [28] [105]. However, the effect of the incidence of a high energy laser with varying scan speeds

on these inoculated composites is not known—an important parameter for full scale part development. Gaps exist in the literature and reported research in how these versatile materials whose grain structure has been improved by inoculation will behave under intense source of heat energy (laser)? What will be the effect on type, size, distribution and morphology of phases as well as size, dimensions and geometries of associated melt pools, heat affected zones and unaffected base material? The present study is aimed to bridge this gap. A systematic study is carried out in which bulk metallic glass matrix composites with different percentages of ZrC subjected to a laser source of constant size (spot size). The effect of laser power and scan speed are evaluated.

2. Experimental Procedure

As cast bulk metallic glass matrix composites are produced using vacuum arc melting and suction casting button furnace. They are produced by mixing appropriate amounts of pure elements Zr, Cu, Al and Co with different percentages of ZrC inoculant such that a small button is produced which is placed in the hearth of furnace and melted with the help of an arc. The melted volume is placed on a small orifice and sucked through a chute into a copper mold beneath using negative pressure generated by a vacuum pump. The sucked volume adopts the shape of copper mold and generates a gradient of microstructure across its length due to the difference in cooling rate. Resulting cast parts are cut from middle of wedge along parting line so that the cut surface having the maximum microstructural features is exposed. One of half is further cut into two small pieces from the middle along the longitudinal direction such that two small strips are produced (**Figure 1**).

Two pieces, one half wedge and one small strip were subjected to laser surface treatment on a Trumpf laser with different parameters. Samples are placed in the enclosed chamber and machine is operated in over pressure of inert gas condition. Three tracks were produced on each of three samples. The first one was made with 500 W power, 0.61 mm spot size and 600 mm/minute scan speed, second one was made with 300 W power, 0.61 mm spot size and 600 mm/minutes can speed while third one was made with 300 W power, 0.61 mm spot size and 1500 mm/minutes can speed. In all three cases, the spot size was kept constant while the power and scan speed were varied to check their effect on final microstructure. An increase in laser power was assumed to exert more energy input, cause more turbulence in the melt pool, increase spatter [3], denudation zones [55] [76], evaporation and distort the surface structure with irregularities (shrinkage, segregation, lapping, cracks, porosity, pin and gas holes [3] [103]) produced during solidification [4] [104] [106] [107].

High laser power is also proposed to induce solid state transformations [108] in solidified melts. These defects are even more pronounced at varying scan speeds and produce range of melt pool geometries [64], shapes and morphologies with a multitude of solidification microstructures. After laser surface treatment, samples were prepared form etallographic examination. A detailed pro-

cedure of melting, casting and metallographic sample preparation can be found in a previous study [109].

Scanning electron microscopy: Back scatter electron microscopy of laser surface treated inoculated samples was performed on a JOEL 7001F FE-SEM equipped with thermally assisted Schottky type field emission gun at the University of New South Wales, Sydney, Australia. Microscope was operated at cathode voltage of 15 KV. Sample was placed in chamber at a vacuum of 10^{-6} mbar created by the diffusion pump connected to it. Secondary electron imaging was performed by a collection of electrons at wall mounted secondary electron (Everhart Thornley type) detector (not shown). Back scatter electron imaging was carried out. These electrons carry information about compositional contrast and clearly identify areas where microstructure is 100% glass, affected by heat (heat affected zone) and remain unaffected and unaltered (base metal). Working distance was maintained at 10.7 ± 0.1 mm.

3. Results and Discussion

Electron microscopy in back scatter imaging mode was performed in all three zones (base metal, heat affected zone and fusion zone) for each and individual track of laser on all three (untreated, inoculated with 0.25% and 0.5% ZrC) $Zr_{47.5}Cu_{45.5}Al_5Co_2$ samples and non-inoculated $Zr_{65}Cu_{15}Al_{10}Ni_{10}$ sample.

3.1. $Zr_{47.5}Cu_{45.5}Al_5Co_2$ (Inoculant = 0%) Track 1

This track is laid with following parameters; Power 500 W, Spot size 0.61, Scan speed 600 mm/min. Three distinct regions may be identified in micrographs of cross section of sample taken at low magnification (Figure 2(a)). These are labelled as A, B and C which may be attributed to Fusion/melt zone, Heat affected zone (HAZ) and untreated/base metal zone respectively. For this sample with given parameters, a very large, wide and deep fusion zone is formed. This is due to very high powers of the laser which cause localised concentration of energy resulting in incipient fusion. At the same power of laser complete melting and

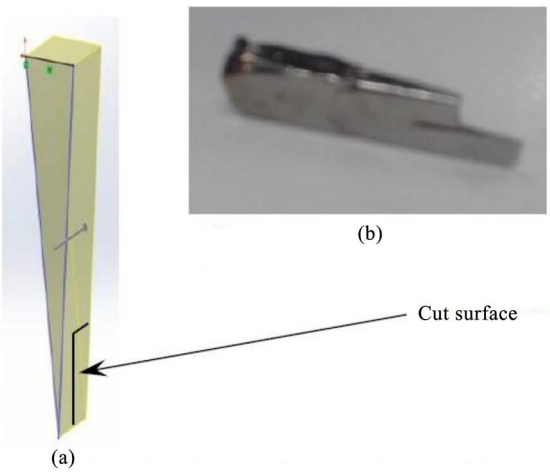

Figure 1. (a) Schematic of wedge shape and cut made on it; (b) Actual cut piece.

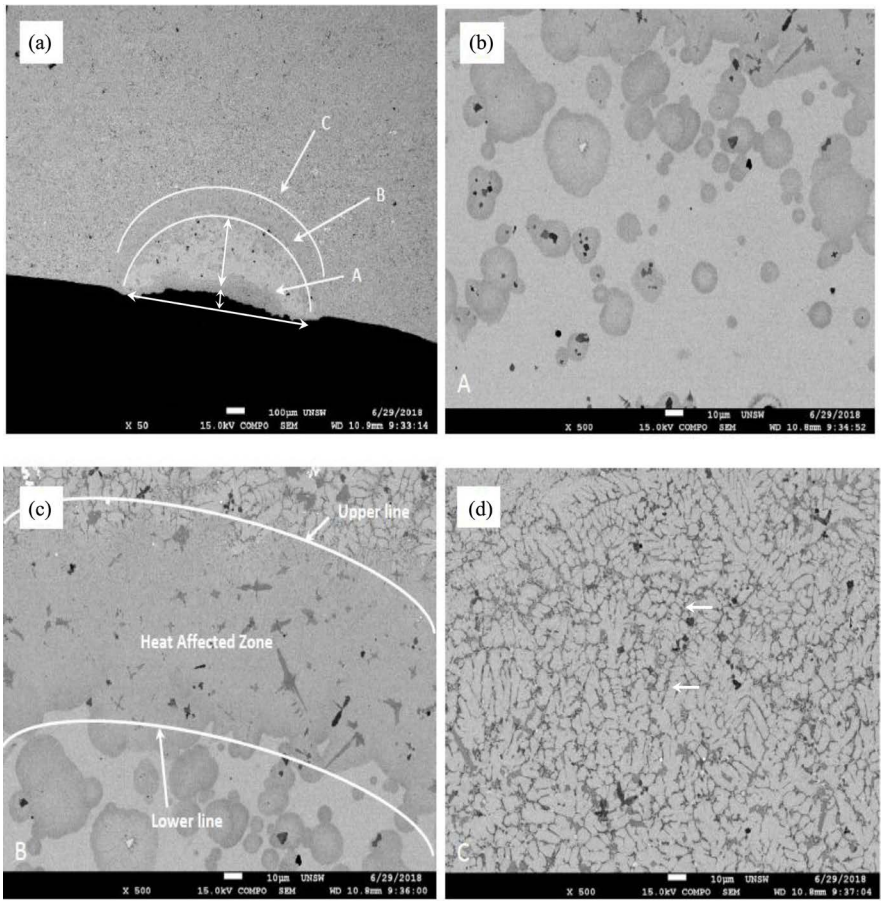

Figure 2. (a)-(d): $Zr_{47.5}Cu_{45.5}Al_5Co_2$ (0% inoculant) Track 1, (a) low magnification (×50) image of cross section of laser track, (b) Back scatter image of fusion zone/melt pool indicating formation of glass and spherulites avoiding nanocrystallites, (c) back scatter image of heat affected zone and (d) back scatter image of base metal indicating presence of different phases (CuZr B2 and small Al_2Zr fcc phase [112]).

rapid solidification of CuZr B2 [20] occurred. This can be observed by the appearance of 100% glassy structure in region A (**Figure 2(b)**).

Another very important characteristic of this zone is formation of spherulites. These are consistent to observations made in a previous study [54] and are in contradiction to nanocrystalline phases observed upon isothermal annealing [110] [111]. Due to the rapid heat extraction and dissipation, these non-equilibrium products are formed. The width of melt pool or fusion zone is approximately 600 μm at the surface while its depth is 300 μm. There is shrinkage of approximately 30 - 40 μm at the top in the middle. Corners or edges of the melt pool are also blurred or torn apart and show signs of deterioration due to intense heat generated by highly localised source of heat (laser). As the point of observation moves away from region A, a region which is depicted by mixed or hazy areas is observed. This is zone where incomplete transformation has occurred, and the structure tends to freeze or coexist as crystalline metastable phase and glassy matrix. This happens as insufficient time is given to allow for complete dissolution of solid to liquid and then from liquid back to solid. This is known as the

heat affected zone (HAZ). As the name suggests, it is region which is affected by heat, but incomplete transformation occurs. Some phases or features are transformed, while others remain untransformed. It appears as distinct region in this sample. The width of this region ranges from 120 - 140 μm. Finally, as the point of observation moves further deep into sample, the base metal or untreated sample is observed (**Figure 2(d)**). This is characterised by observation of well-known and documented spheroidal CuZr B2 phase [20]. There are few small brittle Al_2Zr fcc [112] dendrites emerging from background of glassy liquid. Phases formed are indicated by light colour while glassy matrix appears as dark background. Evidence of small porosity is also observed which appears as areas of black colour indicating empty space.

3.2. $Zr_{47.5}Cu_{45.5}Al_5Co_2$ (Inoculant = 0%) Track 2

This track is produced with following parameters; Power 300 W, Spot size 0.61 mm, Scan speed 600 mm/min. Once again, three distinct regions may be identified in micrographs of cross section of sample taken at low magnification (×50) (**Figure 3(a)**). Once again, these are labelled as A, B and C which are representation off usion/melt zone, heat affected zone (HAZ) and untreated/base metal zone respectfully. For this sample with given parameters, a large, wide and deep fusion/melt zone is observed. This again is due to the high power of the laser which results in concentration of energy causing incipient fusion and formation of melt pool. As the spot size and scan speed are kept constant while laser input power is reduced, it resulted in less deep melt pool. Also, there is less evidence of turbulence caused by reduced power laser. There is some blurring or inconsistency at the top of melt pool but still, it is not as evident as was the case when laser power was 500 W. Some cracking is also observed at the edges of heat affected zone (HAZ). This is due to the difference in temperatures between the melt pool and base metal which causes thermal stresses. Another reason for this may be attributed to emergence of different coefficients of thermal expansion in metal solidified at melt pool (glass) and the composite structure of base metal.

Another phenomenon of interest observed in this track is the emergence of small precipitates in the melt pool region (**Figure 3(b)**). These appear in the form of small equiaxed grains. These may be an indication of incomplete fusion due to the low energy input. Another reason for this, may be attributed to complete melting, freezing and then precipitation of a large number of small equiaxed grains from the glass (recrystallisation/devitrification) due to intense localised heating. There is no evidence of a change inmorphology. Another possibility is that complete fusion occurred and then precipitation of CuZr B2 spheroidal phase from the rapidly solidifying melt. Their size is small as rate of heat extraction from the very small area is very fast resulting in nucleation of large numbers of small grains with suppressed kinetics/growth. As the point of observation moves away from melt pool/fusion zone, a profound heat affected zone (HAZ) is observed in the form of boundary/interface between melt pool and base metal. This region is characterised by an emergence of crystalline phases

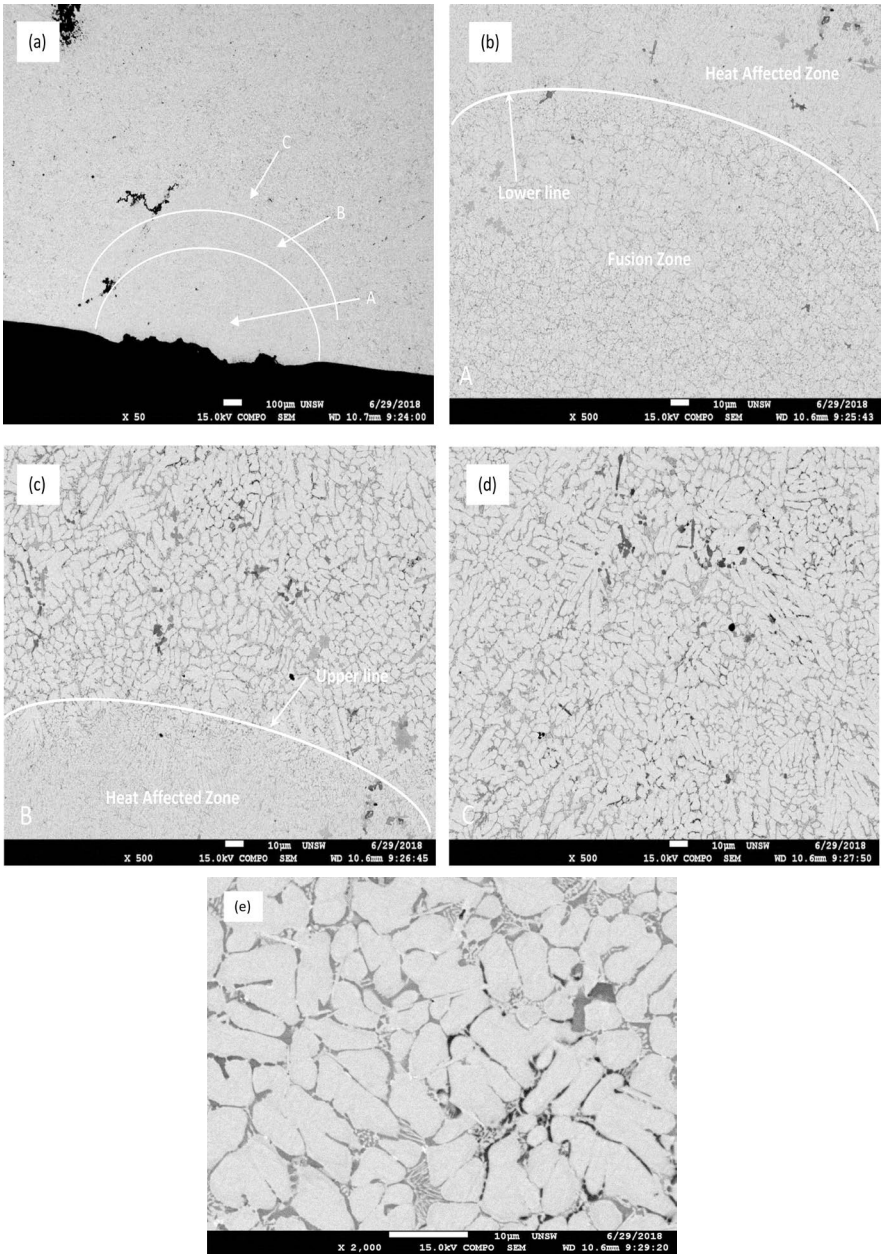

Figure 3. (a)-(e): $Zr_{47.5}Cu_{45.5}Al_5Co_2$ (0% inoculant) Track 2: (a) Low magnification (×50) back scatter image of cross section of laser track, (b) Melt pool and lower region of heat affected zone (×500), (c) Upper region of heat affected zone and its interface with base metal, (d) Back scatter image of base metal indicating presence of CuZr B2 and small Al_2Zr fcc phase [112], (e) base metal at higher magnification (×2500) indicating presence of glassy matrix (dark grey areas)and ductile precipitates (light areas).

and a glassy matrix. However, as the laser power is low, its effect is not as profound as was when power was 500 W. Small cracks were also observed at the edges of the HAZ with base meal. The size of this region is around 120 - 140 µm. Once again, the reason for the cracking may be attributed to difference of temperature or coefficient of thermal expansion between different phases of material. Regular spheroidal shape CuZr B2 [20] precipitates are observed along with

tree/flower like small brittle Al_2Zr fcc phase [112] as the point of observation moves further deep into sample towards base metal zone.

3.3. $Zr_{47.5}Cu_{45.5}Al_5Co_2$ (Inoculant = 0%) Track 3

This track is laid with following parameters; Power 300 W, Spot size 0.61 mm, Scan speed 1500 mm/min. As the power and spot size are kept constant while scan speed is increased, it results in shallower and narrow melt pool or fusion zone as laser tends to move quickly in a given time over an area causing less abrupt action. Consequently, less volume is melted, and only surface effects are observed. There is almost no turbulence and no pronounced effect of shrinkage is observed. Absence of turbulence also promotes homogenisation and fully glassy structure is formed without shrinkage, segregation and appearance of defects caused by movement of melt in confined volume, its interaction with environment (gases and air) and their entrapment. Size of melt pool is approximately 600 μm wide and 350 μm deep. There is small localised depression in the middle of pool which indicates localised shrinkage. As very less volume is melted and the interaction of energy with matter is extremely brief, size of heat affected zone is subsequently decreased and it spans to a maximum width of 100 μm. Considerable decrease in size of heat affected zone indicates effectiveness and suitability of process to develop layer by layer (LBL) patterns as the need of removal of excess unwanted hard material is minimised. Grains in base metal region are mostly uniformly spaced. CuZr B2 tends to retain its near spheroidal morphology but is observed in sparse locations. Most of microstructure is filled with three dimensional small brittle Al_2Zr fcc phase [112] appearing in the form of randomly but uniformly distributed dendrites whose size range from 10 μm to 25 μm (**Figure 4**).

3.4. $Zr_{47.5}Cu_{45.5}Al_5Co_2$ (Inoculant = 0.25%) Track 1

Track produced by incidence of laser on inoculated material surface, subsequent analysis of zones developed, and microstructure evolved in these are explained in **Figure 5(a)-5(d)**. These represent areas where laser energy produces different features on surface of inoculated material. These materials are characterised by presence of certain amount of ZrC inoculant. This imparts grain refinement to material and decreases the size of features (primarily CuZr B2) which can be easily observed in back scatter images of base metal (**Figure 5(d)**). However, effect of laser generates different regions which will be explained in detail below. Laser parameters on this sample are; Power 500 W, Spot size 0.61 mm, Scan speed 600 mm/min. **Figure 5(a)** shows general form and shape of melt pool. It indicates that melt pool is deep and narrow. This is due to intense heat generated by high power laser localised in a confined area. This is backed up with a small spot size and slow scan speed which helps in further confinement of heat in small area increasing the depth to which it can penetrate. Overall width of melt pool and its depth is high as compared to width and depth when material of same composi-

tion without inoculants is subjected to laser surface treatment. Width of melt pool ranges to maximum of 900 μm while its depth extends roughly to 850 μm. Structure of melt pool shows complete fusion, dissolution of all precipitates, homogenisation/mixing, rapid cooling and formation of 100% glassy structure. There is marked indication of cracking due to intense heat generated in a confined area and sharp temperature gradient which exist between fusion zone and neighbouring cold base metal. Cracking may have also been caused due to frictional forces generated during grinding as the material is hard at fusion zone as compared to surrounding and it tends to show resistance to absorb energy and cracks. This crack extends all throughout the volume of material starting from surface towards base metal. Soon after fusion zone, an area depicted by intense effect of heat is witnessed. This is known as heat affected zone (HAZ). This is area which is marked by incomplete/partial transformation. Size of this heat affected zone is very pronounced and profound in this sample. It ranges to maximum of 200 μm wide to 200 μm deep/long. An important feature is observed in this sample. This is presence of small crystals in partial or incomplete transformed

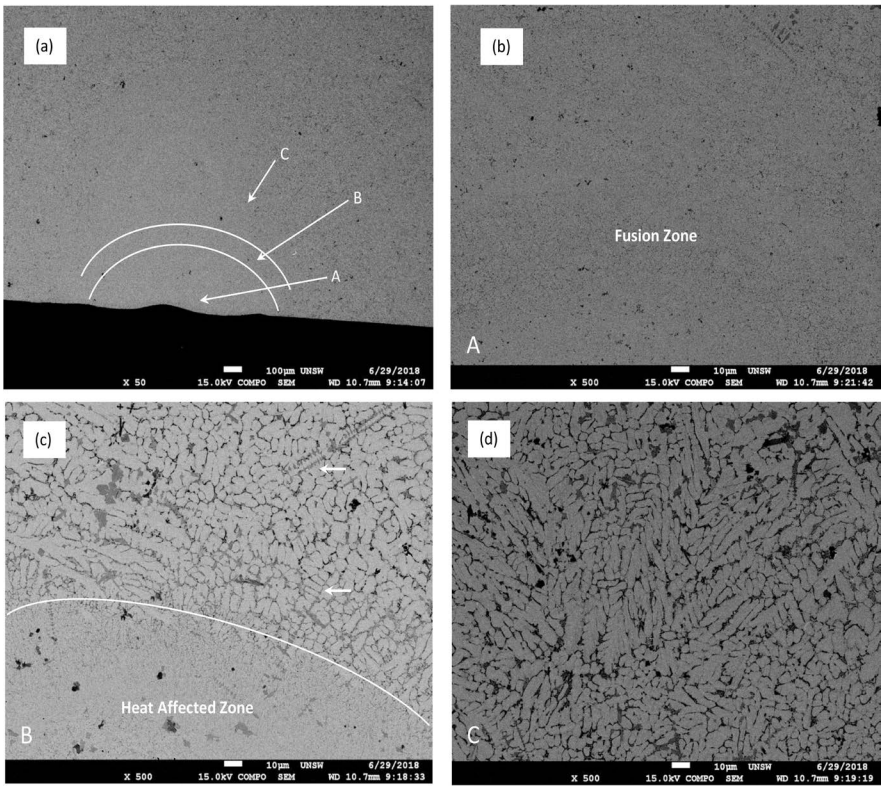

Figure 4. (a)-(d): $Zr_{47.5}Cu_{45.5}Al_5Co_2$ (0% inoculant) Track 3: 300 W, spot size 0.61 mm, Scan speed 1500 mm/min, (a) Low magnification (×50) back scatter electron micrograph of cross section of laser track; (b) Melt pool/fusion zone and lower region of heat affected zone at high magnification indicating complete melting and 100% glassy structure; (c) Upper region of heat affected zone and its interface with base metal; (d) Back scatter image of base metal indicating presence of CuZr B2 and small Al_2Zr fcc phase [112]. Different morphologies of phases can be observed as light areas originating from back ground of glassy matrix (dark areas).

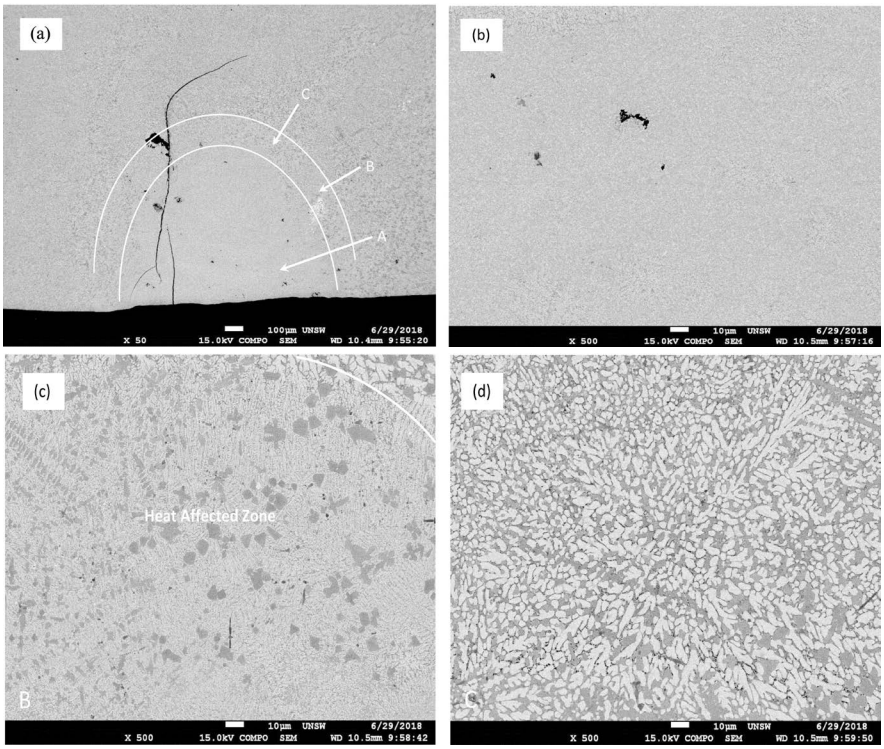

Figure 5. **(a)-(d): $Zr_{47.5}Cu_{45.5}Al_5Co_2$ (0.25% inoculant) Track 1:** Power 500 W, spot size 0.61 mm, scan speed 600 mm/min.

glassy matrix. Appearance of these crystals may also be attributed to inoculation effect itself. As there are stable inoculants present in melt which provide potent sites for heterogeneous nucleation, this sample shows appearance of small crystals even in heat affected zone. Presence of small hairline cracks indicates development of air pockets in solidifying metal. These may have also been caused by shrinkage. Finally, as the point of observation moves away from HAZ towards base metal, microstructure consisting of small precipitates (mainly CuZr B2) emerging out of glassy matrix is observed. This microstructure is characterised by finely dispersed crystals which are present all throughout the matrix. Size of these precipitates/crystals is on average around 2 - 6 µm while their morphology is spheroidal. They are dispersed all throughout the volume of material. They become the source of increase in ductility and toughness of material. There are other small precipitates present in matrix as well bearing dendritic structure which is small brittle Al_2Zr fcc phase [112]. They are consistent with similar structure observed in first glass matrix composite produced by Prof. Johnson's group [39].

3.5. $Zr_{47.5}Cu_{45.5}Al_5Co_2$ (Inoculant = 0.25%) Track 2

As the laser power is reduced while keeping spot size and scan speed constant, structures shown in **Figure 6(a)-6(e)** appear. These clearly show the effect of decrease in laser power which generates less heat and thus causes melting of less amount of material. This in turn generates small melt pool whose size is maxi-

mum 800 μm wide and depth is 450 μm. Decrease in penetration depth is an indication that low power of laser did not generated enough heat at a point to cause deep impression. However, 100% glassy structure is formed and observed in melt pool which is an evidence that amount of heat was enough to cause complete fusion followed by rapid solidification. An important feature shown and observed in this sample is presence of small region in which no melting has occurred. This is characterised by a dark colour spot (Figure 6(b)). This may have been produced because of unmelted ZrC inoculant particle at the centre of growing grain. The grain itself has not grown and may have been frozen due to extremely high cooling rate in a confined volume at the corner of small melt pool. There are few dark spots at top right corner of micrograph which indicate presence of porosity or gas holes. Once again, these may have been caused by poor melt treatment, improper casting practice or improper sample preparation.

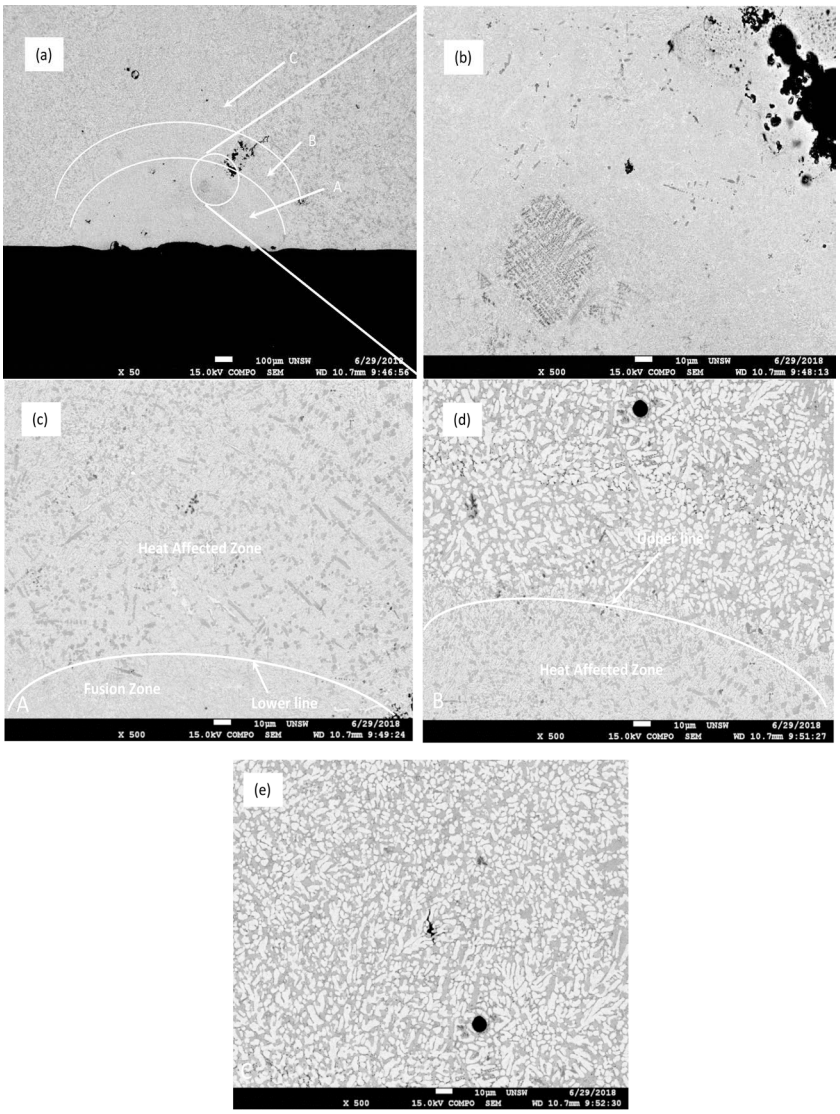

Figure 6. (a)-(e): $Zr_{47.5}Cu_{45.5}Al_5Co_2$ (0.25% inoculant) Track 2: Power 300 W, spot size 0.61 mm, Scan speed 600 mm/min.

As the point of observation moves away from melt pol, once again, an area bearing the effect of intense heat is observed, known as heat affected zone (HAZ) (**Figure 6(c)**). Once again, due to prior inoculation it shows evidence of heterogeneous nucleation in which ductile crystalline particles tend to appear randomly in matrix despite of immense cooling rate observed here. Size of this zone is also very large spanning from approximately 200 μm wide to 250 μm deep. It is marked by a lower and an upper line. Mostly equiaxed grains are observed in this region with a mix of glassy matrix. However, few small columnar grains are observed at the interface of HAZ and base metal. They are formed because of difference of temperature between these two regions and heat transfer occurring as a result (**Figure 6(d)**). Finally, as the point of observation moves to base metal, a microstructure independent of any impulse is witnessed. This is glassy matrix in which number of small CuZr B2 phases is uniformly distributed. Size of these crystalline phases is clearly decreased while their amount has increased. On average, their size is found to be around 1.8 - 2.5 μm. This is evidence of increase in toughness of these alloys which is observed in another study based on microhardness testing described by author elsewhere.

3.6. $Zr_{47.5}Cu_{45.5}Al_5Co_2$ (Inoculant = 0.25%) Track 3

This track is laid out with following parameters; Power: 300 W, Spot size: 0.61 μm, Scan speed: 1500 mm/minutes. Effect of this increased roaster/scan speed at power of 300 W can easily be seen in development of small, shallow and narrow melt pool. Like previous sample, area exhibited by base metal consists of small equiaxed precipitates originating from background of glassy matrix (**Figure 7(d)**). These are mostly equiaxed in nature dispersed evenly all throughout the matrix. Melt/fusion zone on the other hand is manifested by complete fusion and formation of glass (**Figure 7(b)**). There is no evidence of nucleation and growth or precipitation. Area known as heat affected zone (HAZ) which occurs in the middle of glassy matrix and base metal is shown in **Figure 7(c)**. Unlike previous HAZ, the size of this area is reduced to width of almost 200 μm and depth of 180 μm. Primary reason of this is increased scan speed which decreases the time laser spend on metal surface thus creates very short incipient melt pool and associated heat affected zone. Morphology of crystallites in this region is again not quite well developed. However, presence of small Al_2Zr fcc phase [112] can easily be witnessed by appearance of dark areas (near spheroids or sharp needle like precipitates) emerging from the background of glassy matrix. This area is mostly marked by presence of metastable phase. There is almost no evidence of cracking, porosity, pin or gas holes and microstructure mostly shows uniformity.

3.7. $Zr_{47.5}Cu_{45.5}Al_5Co_2$ (Inoculant = 0.5%) Track 1

As the percentage of inoculant increase to 0.5%, a trend marked by increase in number density of phases developed is observed in as cast samples. This is optimistic

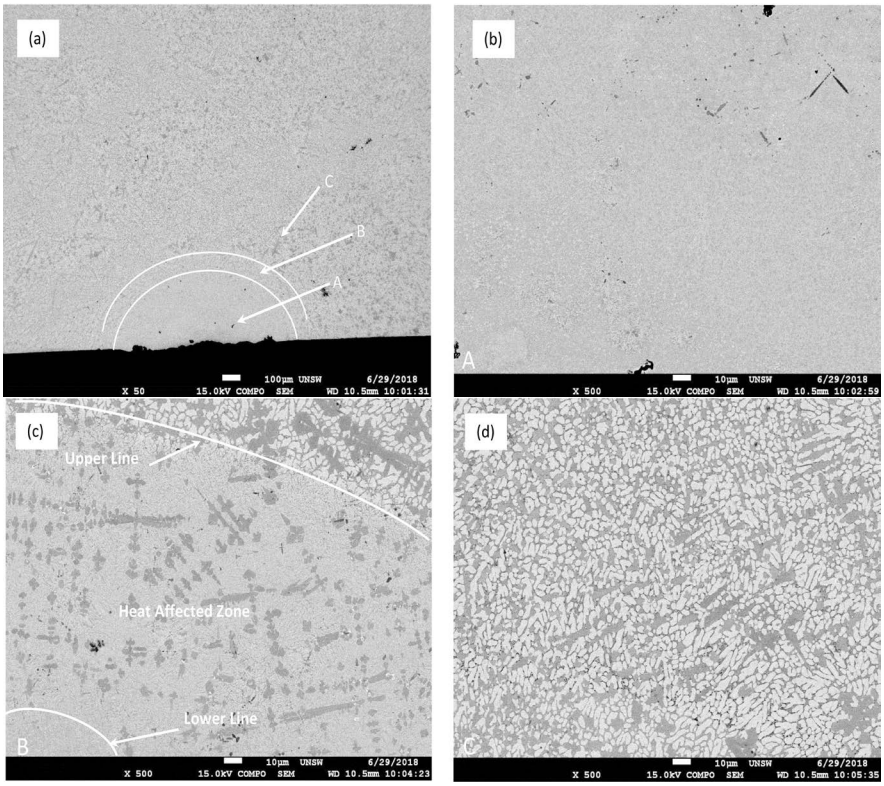

Figure 7. (a)-(d): $Zr_{47.5}Cu_{45.5}Al_5Co_2$ (0.25% inoculant) Track 3: Power 300 W, Spot size 0.61 mm, Scan speed 1500 mm/min.

indicator as a trend marked by increased toughness is expected (as observed by microhardness testing carried out separately described by author elsewhere). However, change in type, size and morphology of same phases as affected by incident laser power is entirely different as will be explained in detail below. **Figure 8(a)** shows low magnification (×50) image of melt pool when laser of 500 W strikes the sample with spot size of 0.61 mm and scan speed of 600 mm/minute. This area is marked by violent and turbulent movement of melt in confined space when it gets melted under the action of intense localised heat. There is a lot of surface roughness and sharp discontinuities on the surface. A marked depression is also observed on the surface indicating profound shrinkage. Total width/span of melt pool is calculated to be around 1000 µm at the surface while its depth is around 550 µm (highest point to bottom). The width of heat affected zone is small and may be calculated to be around 100 µm maximum. One reason which may be attributed to this is combination of speed and laser power. Also, it is anticipated that much of heat in this type of situation will be lost to atmosphere by surface exposure as melt pool is wide. When observed at higher magnification (×500), melt pool shows signs of complete melting followed by rapid solidification characterised by 100% monolithic glassy structure. No evidence of partial or complete crystallisation or recrystallisation is observed in melt pool and microstructure shows no sign of development of any feature (**Figure 8(b)**). Soon after melt pool, an area marked by intense effect of heat on composite is

observed known as heat affected zone (HAZ) (Figure 8(c)). This may be characterised into three regions. 1) Recrystallisedregion (light areas) (mostly these are recrystallised equiaxed CuZr B2 grains), 2) Al_2Zr fcc phase (dark grey areas) [112] and 3) Recrystallised columnar CuZr B2 grains. These are indicated by yellow arrow and found right at the interface/boundary of base metal and heat affected zone carrying equiaxed grains. Finally, when the point of observation moves further away from surface towards base metal, an area unaffected by the heat of laser is observed known as base metal. This is drastically characterised by presence of (a) small equiaxed CuZr B2 phase, glassy matrix (interdendritic dark areas) and Al_2Zr fcc phase (dark grey areas (profound dendritic structure)). There is also evidence of slight interdendritic shrinkage and micro porosity.

3.8. $Zr_{47.5}Cu_{45.5}Al_5Co_2$ (Inoculant = 0.5%) Track 2

Microstructure evolved under the action of decreased power of laser (300 W) with same spot and scan speed is shown in Figures 9(a)-9(e). These are characterised by presence and appearance of typical CuZr B2 phase (spheroidal or near spheroidal), Al_2Zr fcc phase (sharp needle like/flower tip like dark grey areas) [112] and small porosity. Under the action of reduced laser power which generates less heat. Size, shape and morphological features of melt pool are altered and are entirely different. Size of melt pool is decreased, it is manifested by lesser

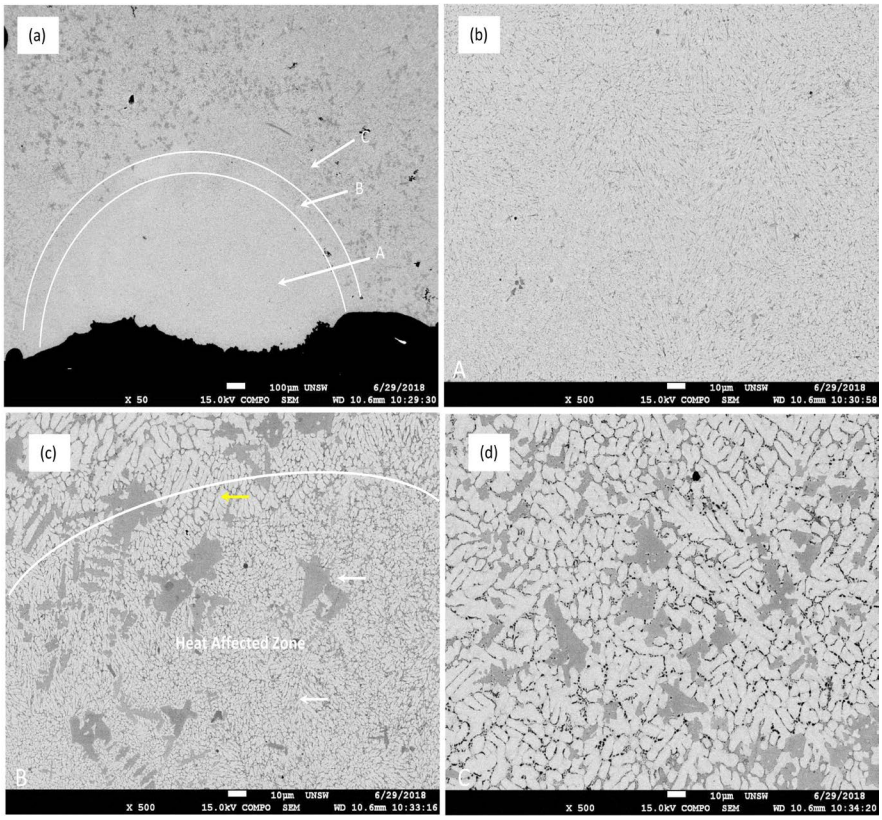

Figure 8. (a)-(d): $Zr_{47.5}Cu_{45.5}Al_5Co_2$ (0.5% inoculant) Track 1: Power 500 W, Spot size 0.61 mm, Scan speed 600 mm/min.

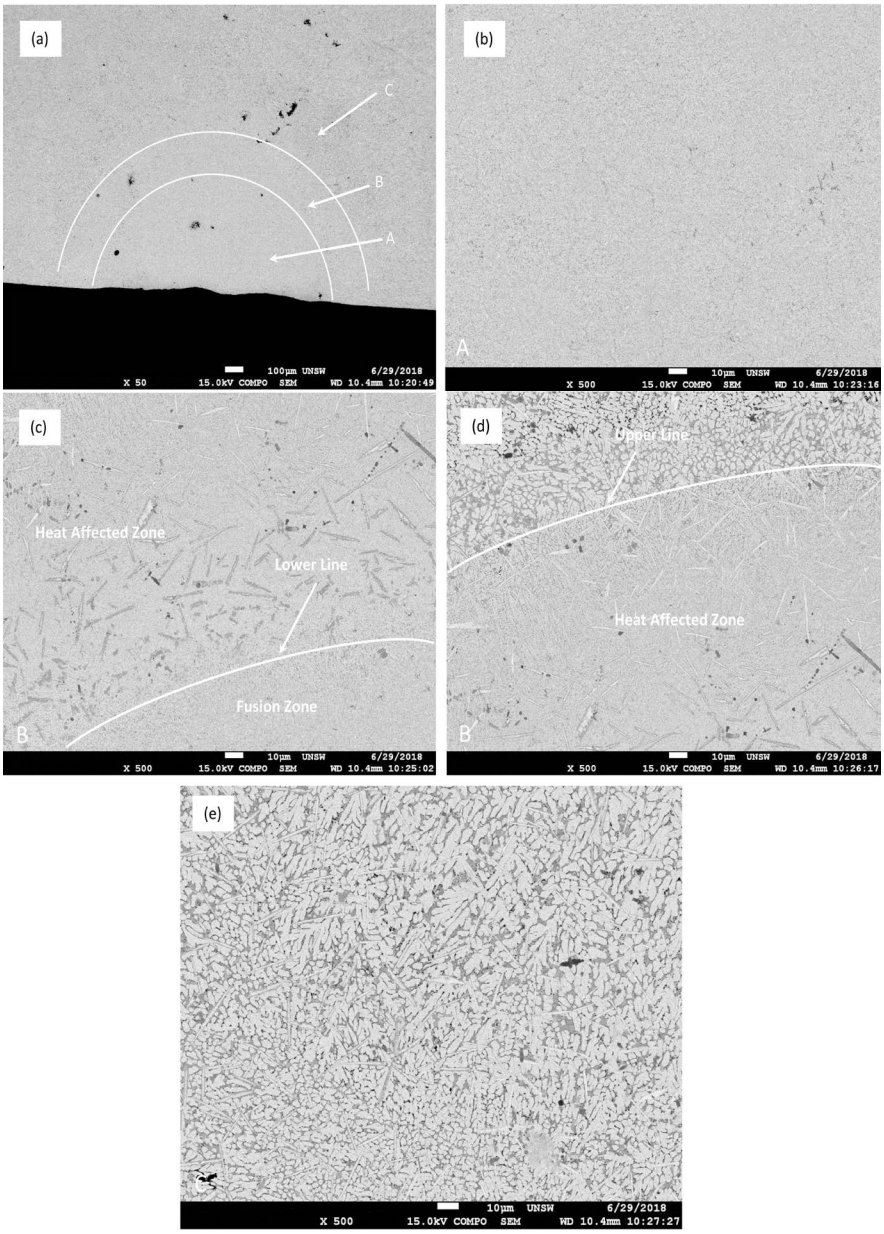

Figure 9. (a)-(e): $Zr_{47.5}Cu_{45.5}Al_5Co_2$ (0.5% inoculant) Track 2: Power 300 W, Spot size 0.61 mm, Scan speed 600 mm/min.

amount of turbulence, hence less spatter, denudation zones and rough corners/edges. There is small evidence of surface depression which indicates shrinkage and small internal porosity. Overall, size/span of melt pool is reduced to 850 - 900 µm at the surface while its depth is also reduced to around 550 µm. An image of melt pool at high magnification (×500) is shown in **Figure 9(b)**. It clearly indicates formation of monolithic 100% glassy structure with no sign or evidence of precipitation. However, as point of observation is moved further deep into sample, an area depicted by partial melting and recrystallisation is observed. This is heat affected zone (**Figure 9(c)**). It clearly shows sign of fusion at certain places and then recrystallisation while some areas specially elongated

Al_2Zr fcc phase are left as such. It appears that CuZr B2 phase is melted completely while Al_2Zr fcc phase experience partial or incomplete melting. Size of heat affected zone is very large spanning to a depth of around 220 - 230 μm. This is shown in two parts in Figures 9(c)-9(d). Base metal with unaltered structure is observed in Figure 9(e). This is marked again with three structures shown and described previously.

3.9. $Zr_{47.5}Cu_{45.5}Al_5Co_2$ (Inoculant = 0.5%) Track 3

Finally, when the scan speed of laser is increased to 1500 mm/minute while keeping laser power at 300 W and spot size at 0.61 mm. Melt pool, heat affected zone (HAZ) and microstructures evolved in these are shown in Figures 10(a)-10(d). Surface of material experience intense effect of heat and there are clear and marked signs of surface roughness, spatter and discontinuities. However, as the laser traverses its path quickly, size of melt pool (both in terms of width and depth) is not very large. It spans at around 70 μm on the surface while its depth is almost similar. There is no indication of precipitation or recrystallization of any phase in melt pool and at higher magnification (×500) (Figure 10(b)). Melt pool depicts placid glassy structure with no crystals. There is however, slight effect of burning at the surface which is characteristic of intense heat. Size of heat affected zone (HAZ) beneath fusion zone is not profound as well. It merely has a depth of around 120 μm. Features observed in this are fused and

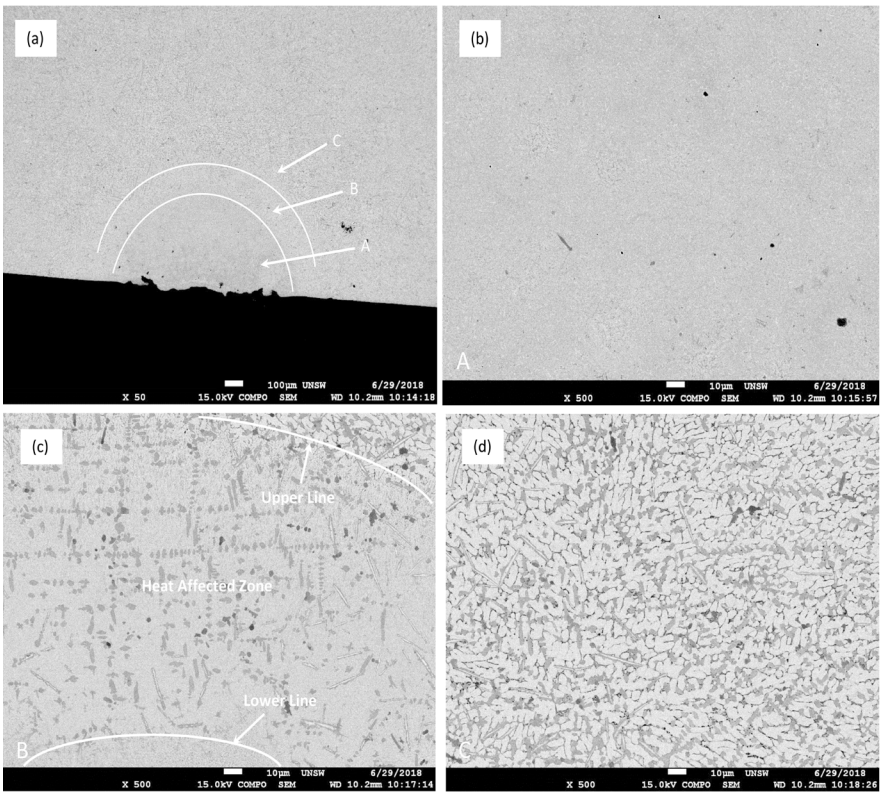

Figure 10. (a)-(d): $Zr_{47.5}Cu_{45.5}Al_5Co_2$ (0.5% inoculant) Track 3: Power 300 W, spot size 0.61 mm, Scan speed 1500 mm/min.

rapidly solidified glass and small brittle Al_2Zr fcc phase. Al_2Zr fcc phase shows tint of silvery or light grey areas typical of this phase as observed previously as well. Surprisingly, there is no observation of spherulites in fusion zone or HAZ of any of inoculated samples (0.25% as well as 0.5%) and it may be inferred that inoculation resists change of morphology. Structure is found in unaltered state in base metal and found to have small to medium size precipitates around 4 - 6 μm in size. Overall effect of intense heat from localised source of energy is found to cast change in microstructure.

3.10. $Zr_{65}Cu_{15}Al_{10}Ni_{10}$ (Inoculant = 0%) Track 1

This track is laid with following parameters. Power 500 W, Spot size 0.61 mm, Scan speed 600 mm/min. At this high-power melt pool is characterized by distinct regions describing complete fusion followed by rapid cooling, turbulent fluid flow, aggressive agitation, discontinuous or broken corners, blurring, inward protrusion or shrinkage, segregation, oxidation and even burning. These are distinctive features of intense heat generated by high power laser in a very small confined volume. A unique feature of this area is burning in the middle of fusion zone. This is due to high heat caused by high power laser. There is thin but continuous white strip all around this burned region indicating rejection of high melting constituents of alloy, oxidation or devitrification. Though, most probable reason for this is oxidation, yet, it is uncommon phenomena observed in these alloys. Exact nature and causes of this are still unknown and further investigation is required before reaching any inference. Almost no porosity is observed in this fusion zone indicating complete melting and fusion followed by rapid cooling which results in formation of glassy structure. Width of this fusion zone at the surface is around 700 μm while its depth is around 600 μm. Maximum depth of shrinkage at the middle of sample is around 200 μm. As the point of observation moves away from this region further deep in to specimen, a region characterized by footprints and effects of heat is observed. This is known as heat affected zone (HAZ). Depth of heat affected zone is very large ranging from 450 - 480 μm. This is indicated by partially melted and fused grains which not only change their size but a considerable change in their morphology is also observed. Mostly equiaxed grains are observed distributed equally all throughout the area of heat affected zone (HAZ).Small footprints of interdendritic shrinkage and porosity are also observed in the form of small black spots. Finally, as the heat affected zone is finished, base metal or region which remains unaltered is observed. This is primarily marked by presence of small to medium size flowery plate like grains of β-Zr. Their size hovers around 100 - 380 μm. Small porosity is also observed specially in grains further away from heat affected zone (**Figure 11**).

3.11. $Zr_{65}Cu_{15}Al_{10}Ni_{10}$ (Inoculant = 0%) Track 2

This track is laid out with reduced power of 300 W while spot size and scan

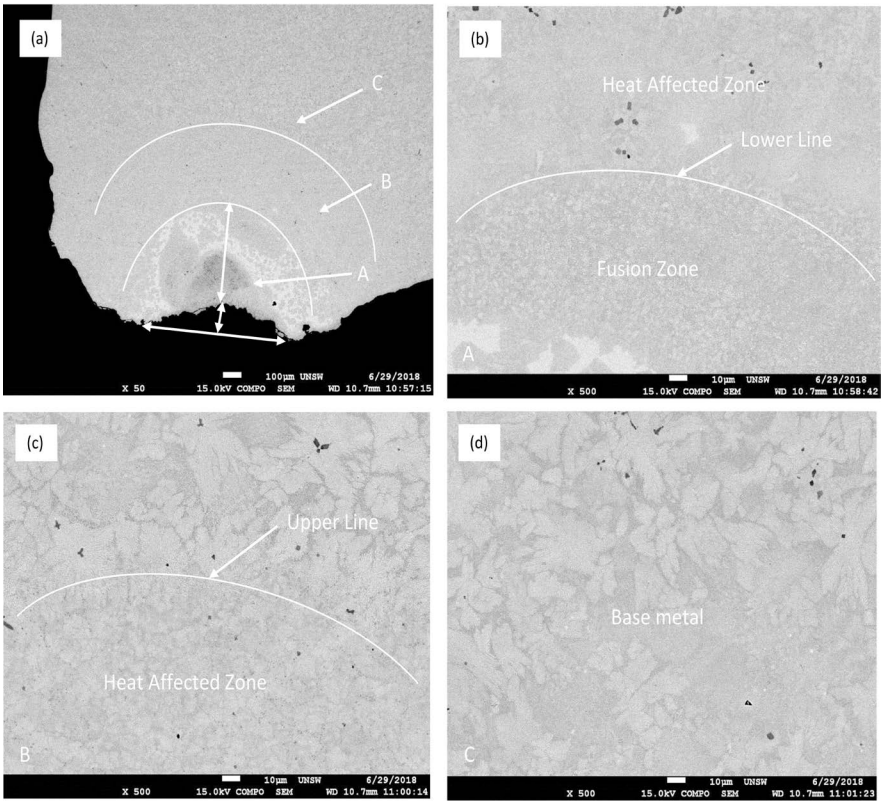

Figure 11. (a)-(d): $Zr_{65}Cu_{15}Al_{10}Ni_{10}$ (inoculant = 0%) Track 1: Power 500 W, spot size 0.61 mm, Scan speed 600 mm/min, (a) Low magnification (×50) back scatter electron micrograph of cross section of laser track; (b) Melt pool/fusion zone and lower region of heat affected zone (HAZ) at high magnification (×500) indicating complete melting and 100% glassy structure. Note: There is no porosity in fusion zone as 100% glass is formed; (c) Upper region of heat affected zone (HAZ) and its interface with base metal; (d) Back scatter image of base metal indicating presence of β-Zr and Zr_2Cu phase [41] [79] [113] [114]. Different morphologies of phases can be observed as light areas originating from back ground of glassy matrix (dark areas).

speed are kept constant at 0.61 mm and 600 mm/min respectively. Once again, three distinct regions may be identified and observed in low magnification (×50) micrograph (**Figure 12(a)**) of cross section of this sample. These are labelled as A, B and C which may be designated as fusion/melt zone, heat affected zone (HAZ) and untreated/base metal zone respectively. Once again, for this sample with given parameters, a very large, wide and deep fusion zone is observed. This is due to still high-power laser with slow scan speed which not only causes localisation of energy in a small confined area but provides enough time for its stay resulting in complete melting/fusion of β-Zr and Zr_2Cu phase [41] [79] [113] [114], turbulent flow, mixing and rapid solidification. This may be observed by the appearance of large 100% glassy structure in region A (**Figure 12(b)**). Once again, large number of small equiaxed grains is observed in fusion zone. These may have been caused by complete melting, solidification and then precipitation of many small equiaxed grains from the glass (recrystallisation/devitrification). There is no evidence ofa change in morphology. Another possibility is complete

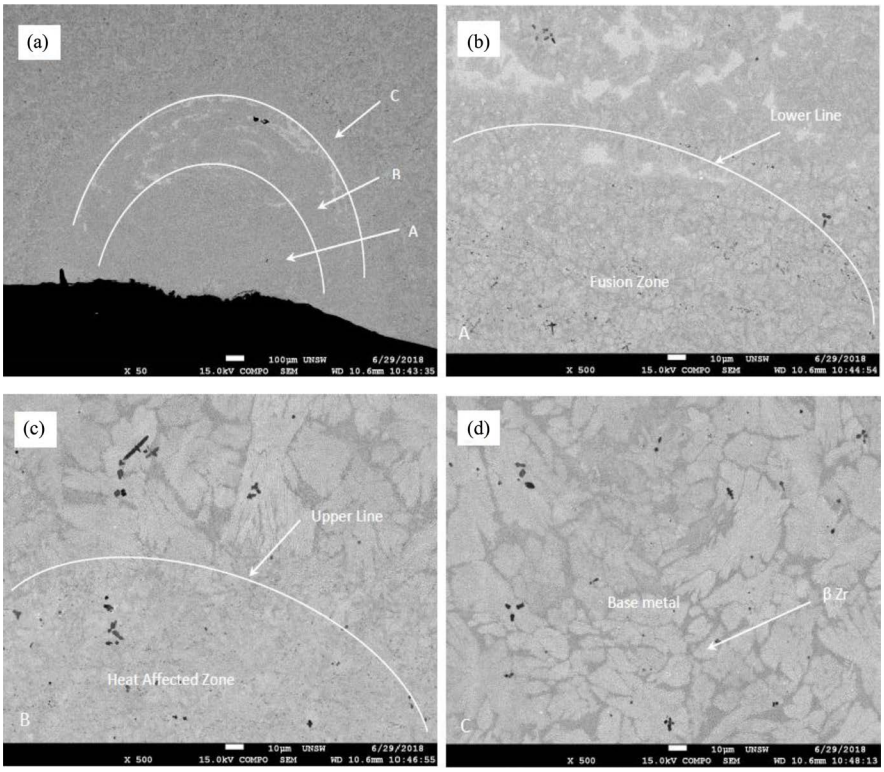

Figure 12. (a)-(d): $Zr_{65}Cu_{15}Al_{10}Co_{10}$ (0% inoculant) Track 2, (a) low magnification (×50) image of cross section of laser track; (b) Back scatter image of fusion zone/melt pool indicating formation of glass; (c) back scatter image of heat affected zone and (d) back scatter image of base metal indicating presence of different phases (β-Zr and Zr_2Cu phase [41] [79] [113] [114]).

fusion followed by *in-situ* precipitation of β-Zr and Zr_2Cu phase from the rapidly solidifying melt. Their type is mostly fine equiaxed grains and size is around 2 - 4 μm. The width of melt pool or fusion zone is approximately 720 μm at the surface while its depth is around 500 μm. There is an indication of small outward protrusion in the middle of sample. No visible or profound shrinkage is observed. White areas indicating segregation have disappeared and have transformed into small streaks spread radially along curvature of heat affected zone (**Figure 12(c)**). Width of heat affected zone (HAZ) ranges from 180 - 200 μm. Finally, as the point of observation moves further deep into sample, base metal or unaffected sample is observed (**Figure 12(d)**). This is characterised by observation of well-known and documented β-Zr and Zr_2Cu phases [41] [79] [113] [114]. Their type (morphology) varies from small equiaxed to large plates with high aspect ratio as rate of heat extraction from very small area varies from very fast→medium→slow. Their size varies from 6 μm to 20 μm. Evidence of small porosity is also observed which appears as areas of black colour indicating empty space.

3.12. $Zr_{65}Cu_{15}Al_{10}Co_{10}$ (Inoculant = 0%) Track 3

This track is laid out with following parameters; Power 300 W, Spot size 0.61

mm and Scan speed 1500 mm/min. Once again, three distinct regions labelled as A, B and Cindicating fusion/melt zone, heat affected zone (HAZ) and untreated/base metal zone respectfully are observed in low magnification (×50) micrograph (Figure 13(a)). For this sample with given parameters, a large, wide and shallow fusion/melt zone is observed. This is marked by profound and distinct inward protrusion or depression indicating major shrinkage. Melt pool is shallow as laser power is not too high. Corners of melt pool indicate marked discontinuities, blurring or broken edges which is due to turbulence caused by localised source of heat energy. No grains are observed in melt pool as complete melting/fusion results in formation of 100% glass. White region again appears in the form of small continuous thin boundary layer at the interface of melt pool ad heat affected zone. This may have been formed by segregation of elements during solidification. Another reason could have been formation of an intermetallic. This may have also been an effect of action of sample preparation fluids on surface of material. Yet, another reason for its formation could have been surface oxidation. However, no evidence of surface oxidation has been witnessed in any previous study. These alloys are amenable to selective dissolution [28] [53] [115] [116] but surface oxidation is rarely observed. Evidence of small porosity is also

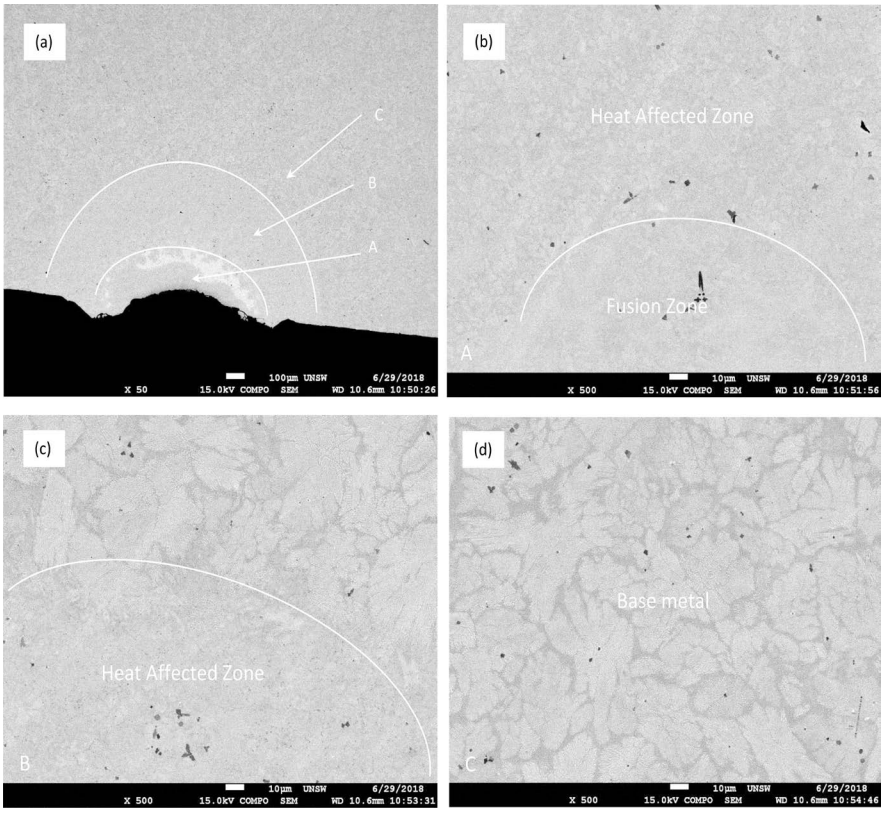

Figure 13. (a)-(d): $Zr_{65}Cu_{15}Al_{10}Co_{10}$ (0% inoculant) Track 3: (a) Low magnification (×50) back scatter image of cross section of laser track; (b) Melt pool and lower region of heat affected zone (×500); (c) Upper region of heat affected zone and its interface with base metal; (d) Back scatter image of base metal indicating presence of β-Zr and Zr_2Cu phase [41] [79] [113] [114].

witnessed at the centre of melt pool or fusion zone (Figure 12(b)). As the point of observation moves away from fusion zone, heat affected zone (HAZ) is observed. Depth of heat affected zone (HAZ) in this sample is around 400 μm in a line along the midpoint of sample while it decreases to around 300 μm at the edges. Small porosity is also observed in HAZ. Soon after HAZ, base metal appears which mostly remains unaltered throughout the specimen. Size of β-Zr plates increases many times as compared to when laser power was very high indicating steady state heat transfer (because time laser spend on material is very low). There is very small cracking at the corners of melt pool indicating presence of thermal gradient between cold base metal and hot fusion zone.

4. Conclusions

In general, following conclusions could be drawn:

1) Inoculation treatment cast an effect of refinement on microstructure (type, size, nature, amount (volume fraction) and distribution of phases).
2) ZrC is found to be an effective new inoculant for bulk metallic glass matrix composites.
3) As the percentage of inoculant increase from zero to 0.5%, type, size, shape and morphology of phases change and their amount increase.
4) Size of CuZr B2 phase gets refined and decrease from around 4 μm to 2.8 μm with increase of percentage of inoculant from zero to 0.25% while increase slightly when percentage of inoculant increase to 0.5% indicating non-linearity.
5) Another phase namely brittle Al_2Zr fcc phase (small to medium columnar dendrites) is also observed to form out of glassy melt.
6) Morphology of CuZr B2 change from spheroids to spherulite under the effect of intense heat observed only when laser power is 500 W and there is no inoculation.
7) Inoculation is found to resist change of morphology of phases in melted and rapidly solidified material as no evidence of spherulites is observed in samples treated with ZrC.
8) Evidence of steady state heat transfer is observed in $Zr_{65}Cu_{15}Al_{10}Co_{10}$ without any inoculant witnessed by various size and morphology of β-Zr and Zr_2Cu phases [41] [79] [113] [114].

Acknowledgements

Authors would like to thank Dr. Daniel East (CSIRO) for providing experimental facilities for melting and casting of samples, Dr. Dong Qiu for design of inoculants and providing their samples, Mr. Alan Jones (Additive Manufacturing Precinct, RMIT University) for performing laser surface treatment, Mr. Jeremy Gonzalez (Massachusetts Materials Research Inc., Worcester, MA) for cutting, mounting, grinding and polishing of samples and Dr. Simon Hager (University of New South Wales, Sydney) for help in performing scanning electron microscopy in back scatter electron imaging mode. Lead author would also like to

thank Prof. Milan Brandt (also author) for moral support, patience, helpful scientific discussion and guidance and RMIT University for providing stipend for tuition and living.

Conflicts of Interest

The authors declare no conflicts of interest regarding the publication of this paper.

References

[1] Avner, S.H. (1974) Introduction to Physical Metallurgy. McGraw-Hill, New York, NY.

[2] Porter, D.A. and Easterling, K.E. (1992) Phase Transformations in Metals and Alloys. 3rd Edition, Taylor & Francis, Milton Park, UK. https://doi.org/10.1007/978-1-4899-3051-4

[3] Taylor, H.F. (1959) Foundry Engineering. Wiley, Hoboken, NJ.

[4] Kurz, W. and Fisher, D.J. (1986) Fundamentals of Solidification. Trans Tech Publications, Zurich, Switzerland.

[5] Klement, W., Willens, R.H. and Duwez, P.O.L. (1960) Non-Crystalline Structure in Solidified Gold-Silicon Alloys. *Nature*, **187**, 869-870. https://doi.org/10.1038/187869b0

[6] Telford, M. (2004) The Case for Bulk Metallic Glass. *Materials Today*, **7**, 36-43. https://doi.org/10.1016/S1369-7021(04)00124-5

[7] Chen, M. (2011) A Brief Overview of Bulk Metallic Glasses. *NPG Asia Materials*, **3**, 82-90. https://doi.org/10.1038/asiamat.2011.30

[8] Schroers, J. and Johnson, W.L. (2004) Ductile Bulk Metallic Glass. *Physical Review Letters*, **93**, Article ID: 255506. https://doi.org/10.1103/PhysRevLett.93.255506

[9] Greer, A.L. (1995) Metallic Glasses. *Science*, **267**, 1947-1953. https://doi.org/10.1126/science.267.5206.1947

[10] Güntherodt, H.J. (1977) Metallic Glasses. In: Treusch, J., Ed., *Festkörperprobleme 17: Plenary Lectures of the Divisions "Semiconductor Physics" "Metal Physics" "Low Temperature Physics" "Thermodynamics and Statistical Physics" "Crystallography" "Magnetism" "Surface Physics" of the German Physical Society Münster*, Springer, Berlin, Heidelberg, 25-53.

[11] Ashby, M.F. and Greer, A.L. (2006) Metallic Glasses as Structural Materials. *Scripta Materialia*, **54**, 321-326. https://doi.org/10.1016/j.scriptamat.2005.09.051

[12] Si, J.J., *et al.* (2015) Cr-Based Bulk Metallic Glasses with Ultrahigh Hardness. *Applied Physics Letters*, **106**, Article ID: 251905. https://doi.org/10.1063/1.4923210

[13] Ramamurty, U., *et al.* (2005) Hardness and Plastic Deformation in a Bulk Metallic glass. *Acta Materialia*, **53**, 705-717. https://doi.org/10.1016/j.actamat.2004.10.023

[14] Greer, A.L., Cheng, Y.Q. and Ma, E. (2013) Shear Bands in Metallic Glasses. *Materials Science and Engineering: R: Reports*, **74**, 71-132. https://doi.org/10.1016/j.mser.2013.04.001

[15] Yang, Y. and Liu, C.T. (2012) Size Effect on Stability of Shear-Band Propagation in Bulk Metallic Glasses: An Overview. *Journal of Materials Science*, **47**, 55-67. https://doi.org/10.1007/s10853-011-5915-8

[16] Packard, C.E. and Schuh, C.A. (2007) Initiation of Shear Bands near a Stress Con-

centration in Metallic Glass. *Acta Materialia*, **55**, 5348-5358. https://doi.org/10.1016/j.actamat.2007.05.054

[17] Zhu, Z., *et al.* (2010) Ta-Particulate Reinforced Zr-Based Bulk Metallic Glass Matrix Composite with Tensile Plasticity. *Scripta Materialia*, **62**, 278-281. https://doi.org/10.1016/j.scriptamat.2009.11.018

[18] Fan, C., *et al.* (2006) Mechanical Behavior of Bulk Amorphous Alloys Reinforced by Ductile Particles at Cryogenic Temperatures. *Physical Review Letters*, **96**, Article ID: 145506. https://doi.org/10.1103/PhysRevLett.96.145506

[19] Choi-Yim, H., *et al.* (2002) Processing, Microstructure and Properties of Ductile metal Particulate Reinforced $Zr_{57}Nb_5Al_{10}Cu_{15.4}Ni_{12.6}$ Bulk Metallic Glass Composites. *Acta Materialia*, **50**, 2737-2745. https://doi.org/10.1016/S1359-6454(02)00113-1

[20] Liu, J., *et al.* (2010) In Situ Spherical B2 CuZr Phase Reinforced ZrCuNiAlNb Bulk Metallic Glass Matrix Composite. *Journal of Materials Research*, **25**, 1159-1163. https://doi.org/10.1557/JMR.2010.0138

[21] Fan, C., Ott, R.T. and Hufnagel, T.C. (2002) Metallic Glass Matrix Composite with Precipitated Ductile Reinforcement. *Applied Physics Letters*, **81**, 1020-1022. https://doi.org/10.1063/1.1498864

[22] Jiang, F., *et al.* (2007) Microstructure Evolution and Mechanical Properties of $Cu_{46}Zr_{47}Al_7$ Bulk Metallic Glass Composite Containing CuZr Crystallizing Phases. *Materials Science and Engineering*: *A*, **467**, 139-145. https://doi.org/10.1016/j.msea.2007.02.093

[23] Chen, G., *et al.* (2009) Enhanced Plasticity in a Zr-Based Bulk Metallic Glass Composite with *in Situ* Formed Intermetallic Phases. *Applied Physics Letters*, **95**, Article ID: 081908. https://doi.org/10.1063/1.3211912

[24] Guo, W. and Kato, H. (2015) Development and Microstructure Optimization of Mg-Based Metallic Glass Matrix Composites with in Situ B2-NiTi Dispersoids. *Materials & Design*, **83**, 238-248. https://doi.org/10.1016/j.matdes.2015.06.033

[25] Jeon, C., *et al.* (2015) Effects of Effective Dendrite Size on Tensile Deformation Behavior in Ti-Based Dendrite-Containing Amorphous Matrix Composites Modified from Ti-6Al-4V Alloy. *Metallurgical and Materials Transactions A*, **46**, 235-250. https://doi.org/10.1007/s11661-014-2531-7

[26] Zhang, T., *et al.* (2014) Dendrite Size Dependence of Tensile Plasticity of *in Situ* Ti-Based Metallic Glass Matrix Composites. *Journal of Alloys and Compounds*, **583**, 593-597. https://doi.org/10.1016/j.jallcom.2013.08.201

[27] Hofmann, D.C., *et al.* (2016) Castable Bulk Metallic Glass Strain Wave Gears: Towards Decreasing the Cost of High-Performance Robotics. *Scientific Reports*, **6**, 3 Article ID: 7773. https://doi.org/10.1038/srep37773

[28] Rafique, M.M.A. (2018) Production and Characterization of Zr Based Bulk Metallic Glass Matrix Composites (BMGMC) in the Form of Wedge Shape Ingots. *Engineering*, **10**, 215-245. https://doi.org/10.4236/eng.2018.104015

[29] Kim, D.H., *et al.* (2013) Phase Separation in Metallic Glasses. Progress in Materials. *Science*, **58**, 1103-1172. https://doi.org/10.1016/j.pmatsci.2013.04.002

[30] Basu, J., *et al.* (2003) Microstructure and Mechanical Properties of a Partially Crystallized La-Based Bulk Metallic Glass. *Philosophical Magazine*, **83**, 1747-1760. https://doi.org/10.1080/01418618610310001041 63

[31] Taub, A.I. and Spaepen, F. (1980) The Kinetics of Structural Relaxation of a Metallic glass. *Acta Metallurgica*, **28**, 1781-1788. https://doi.org/10.1016/0001-6160(80)90031-0

[32] Zhang, Y., Wang, W.H. and Greer, A.L. (2006) Making Metallic Glasses Plastic by Control of Residual Stress. *Nature Materials*, **5**, 857-860. https://doi.org/10.1038/nmat1758

[33] Fan, C., *et al.* (2006) Properties of As-Cast and Structurally Relaxed Zr-Based Bulk Metallic Glasses. *Journal of Non-Crystalline Solids*, **352**, 174-179. https://doi.org/10.1016/j.jnoncrysol.2005.11.016

[34] Krämer, L., Champion, Y. and Pippan, R. (2017) From Powders to Bulk Metallic Glass Composites. *Scientific Reports*, **7**, 6651. https://doi.org/10.1038/s41598-017-06424-4

[35] Brothers, A.H. and Dunand, D.C. (2005) Ductile Bulk Metallic Glass Foams. *Advanced Materials*, **17**, 484-486. https://doi.org/10.1002/adma.200400897

[36] Liu, Z., *et al.* (2012) Pronounced Ductility in CuZrAl Ternary Bulk Metallic Glass Composites with Optimized Microstructure through Melt Adjustment. *AIP Advances*, **2**, Article ID: 032176. https://doi.org/10.1063/1.4754853

[37] Cheng, J.-L., *et al.* (2013) Innovative Approach to the Design of Low-Cost Zr-Based BMG Composites with Good Glass Formation. *Scientific Reports*, **3**, 2097. https://doi.org/10.1038/srep02097

[38] Harooni, A., *et al.* (2016) Processing Window Development for Laser Cladding of Zirconium on Zirconium Alloy. *Journal of Materials Processing Technology*, **230**, 263-271. https://doi.org/10.1016/j.jmatprotec.2015.11.028

[39] Hays, C.C., Kim, C.P. and Johnson, W.L. (2000) Microstructure Controlled Shear Band Pattern Formation and Enhanced Plasticity of Bulk Metallic Glasses Containing *in Situ* Formed Ductile Phase Dendrite Dispersions. *Physical Review Letters*, **84**, 2901-2904. https://doi.org/10.1103/PhysRevLett.84.2901

[40] Scudino, S., *et al.* (2011) Ductile Bulk Metallic Glasses Produced through Designed Heterogeneities. *Scripta Materialia*, **65**, 815-818. https://doi.org/10.1016/j.scriptamat.2011.07.039

[41] Gargarella, P., *et al.* (2014) Phase Formation and Mechanical Properties of Ti-Cu-Ni-Zr Bulk Metallic Glass Composites. *Acta Materialia*, **65**, 259-269. https://doi.org/10.1016/j.actamat.2013.10.068

[42] Das, J., *et al.* (2005) "Work-Hardenable" Ductile Bulk Metallic Glass. *Physical Review Letters*, **94**, Article ID: 205501. https://doi.org/10.1103/PhysRevLett.94.205501

[43] Das, J., *et al.* (2007) Plasticity in Bulk Metallic Glasses Investigated via the Strain Distribution. *Physical Review B*, **76**, Article ID: 092203. https://doi.org/10.1103/PhysRevB.76.092203

[44] Kim, K.B., *et al.* (2005) Heterogeneous Distribution of Shear Strains in Deformed $Ti_{66.1}Cu_8Ni_{4.8}Sn_{7.2}Nb_{13.9}$ Nanostructure-Dendrite Composite. *Physica Status Solidi* (*a*), **202**, 2405-2412. https://doi.org/10.1002/pssa.200520073

[45] Fan, C., Li, C. and Inoue, A. (2000) Nanocrystal Composites in Zr-Nb-Cu-Al Metallic Glasses. *Journal of Non-Crystalline Solids*, **270**, 28-33. https://doi.org/10.1016/S0022-3093(00)00078-8

[46] Inoue, A., *et al.* (2015) Production Methods and Properties of Engineering Glassy Alloys and Composites. *Intermetallics*, **58**, 20-30. https://doi.org/10.1016/j.intermet.2014.11.001

[47] Hofmann, D.C., *et al.* (2008) Designing Metallic Glass Matrix Composites with High Toughness and Tensile Ductility. *Nature*, **451**, 1085-1089. https://doi.org/10.1038/nature06598

[48] Hofmann, D.C., *et al.* (2008) Development of Tough, Low-Density Titanium-Based

Bulk Metallic Glass Matrix Composites with Tensile Ductility. *Proceedings of the National Academy of Sciences*, **105**, 20136-20140. https://doi.org/10.1073/pnas.0809000106

[49] Zhang, L., *et al.* (2017) Distribution of Be in a Ti-Based Bulk Metallic Glass Composite Containing B-Ti. *Journal of Materials Science & Technology*, **33**, 708-711. https://doi.org/10.1016/j.jmst.2016.03.025

[50] Booth, J., Lewandowski, J. and Carter, J. (2014) EBSD Analysis for Microstructure Characterization of Zr-based Bulk Metallic Glass Composites. *Microscopy and Microanalysis*, **20**, 852-853. https://doi.org/10.1017/S1431927614005984

[51] Hofmann, D.C. and Johnson, W.L. (2010) Improving Ductility in Nanostructured Materials and Metallic Glasses: "Three Laws". In: *Materials Science Forum*, Trans Tech Publications, Zurich, Switzerland.

[52] Jiang, J.-Z., *et al.* (2015) Low-Density High-Strength Bulk Metallic Glasses and Their Composites: A Review. *Advanced Engineering Materials*, **17**, 761-780. https://doi.org/10.1002/adem.201400252

[53] Qiao, J., Jia, H. and Liaw, P.K. (2016) Metallic Glass Matrix Composites. *Materials Science and Engineering*: *R*: *Reports*, **100**, 1-69. https://doi.org/10.1016/j.mser.2015.12.001

[54] Sun, H. and Flores, K.M. (2010) Microstructural Analysis of a Laser-Processed Zr-Based Bulk Metallic Glass. *Metallurgical and Materials Transactions A*, **41**, 1752-1757. https://doi.org/10.1007/s11661-009-0151-4

[55] Rafique, M.M.A. (2018) Modelling and Simulation of Solidification Phenomena during Additive Manufacturing of Bulk Metallic Glass Matrix Composites (BMGMC): A Brief Review and Introduction of Technique. *Journal of Encapsulation and Adsorption Sciences*, **8**, 50.

[56] Park, E.S. and Kim, D.H. (2005) Design of Bulk Metallic Glasses with High Glass Forming Ability and Enhancement of Plasticity in Metallic Glass Matrix Composites: A Review. *Metals and Materials International*, **11**, 19-27. https://doi.org/10.1007/BF03027480

[57] Gibson, I., Rosen, W.D. and Stucker, B. (2010) Development of Additive Manufacturing Technology, in Additive Manufacturing Technologies: Rapid Prototyping to Direct Digital Manufacturing. Springer, Boston, MA, 36-58. https://doi.org/10.1007/978-1-4419-1120-9_2

[58] Frazier, W.E. (2014) Metal Additive Manufacturing: A Review. *Journal of Materials Engineering and Performance*, **23**, 1917-1928. https://doi.org/10.1007/s11665-014-0958-z

[59] Sames, W.J., *et al.* (2016) The Metallurgy and Processing Science of Metal Additive manufacturing. *International Materials Reviews*, **61**, 315-360. https://doi.org/10.1080/09506608.2015.1116649

[60] Wong, K.V. and Hernandez, A. (2012) A Review of Additive Manufacturing. *ISRN Mechanical Engineering*, **2012**, Article ID: 208760. https://doi.org/10.5402/2012/208760

[61] DebRoy, T., *et al.* (2018) Additive Manufacturing of Metallic Components—Process, Structure and Properties. *Progress in Materials Science*, **92**, 112-224. https://doi.org/10.1016/j.pmatsci.2017.10.001

[62] Yap, C.Y., *et al.* (2015) Review of Selective Laser Melting: Materials and Applications. *Applied Physics Reviews*, **2**, Article ID: 041101. https://doi.org/10.1063/1.4935926

[63] Zheng, B., *et al.* (2008) Thermal Behavior and Microstructural Evolution during

Laser Deposition with Laser-Engineered Net Shaping: Part I. Numerical Calculations. *Metallurgical and Materials Transactions A*, **39**, 2228-2236. https://doi.org/10.1007/s11661-008-9557-7

[64] Romano, J., *et al.* (2015) Temperature Distribution and Melt Geometry in Laser and Electron-Beam Melting Processes—A Comparison among Common Materials. *Additive Manufacturing*, **8**, 1-11. https://doi.org/10.1016/j.addma.2015.07.003

[65] Gong, X. and Chou, K. (2015) Phase-Field Modeling of Microstructure Evolution in Electron Beam Additive Manufacturing. *JOM*, **67**, 1176-1182. https://doi.org/10.1007/s11837-015-1352-5

[66] Zhang, Y., *et al.* (2015) Microstructural Analysis of $Zr_{55}Cu_{30}Al_{10}Ni_5$ Bulk Metallic Glasses by Laser Surface Remelting and Laser Solid Forming. *Intermetallics*, **66**, 22-30. https://doi.org/10.1016/j.intermet.2015.06.007

[67] Olakanmi, E.O., Cochrane, R.F. and Dalgarno, K.W. (2015) A Review on Selective laser Sintering/Melting (SLS/SLM) of Aluminium Alloy Powders: Processing, Microstructure, and Properties. *Progress in Materials Science*, **74**, 401-477. https://doi.org/10.1016/j.pmatsci.2015.03.002

[68] Li, X.P., *et al.* (2016) Selective Laser Melting of Zr-Based Bulk Metallic Glasses: Processing, Microstructure and Mechanical Properties. *Materials & Design*, **112**, 217-226. https://doi.org/10.1016/j.matdes.2016.09.071

[69] Yang, G., *et al.* (2012) Laser solid forming Zr-based bulk metallic glass. *Intermetallics*, **22**, 110-115. https://doi.org/10.1016/j.intermet.2011.10.008

[70] Welk, B.A., *et al.* (2014) Phase Selection in a Laser Surface Melted Zr-Cu-Ni-Al-Nb Alloy. *Metallurgical and Materials Transactions B*, **45**, 547-554. https://doi.org/10.1007/s11663-013-9907-8

[71] Cardinal, S., *et al.* (2018) Manufacturing of Cu-Based Metallic Glasses Matrix Composites by Spark Plasma Sintering. *Materials Science and Engineering*: *A*, **711**, 405-414. https://doi.org/10.1016/j.msea.2017.11.052

[72] Buchbinder, D., *et al.* (2011) High Power Selective Laser Melting (HP SLM) of Aluminum Parts. *Physics Procedia*, **12**, 271-278. https://doi.org/10.1016/j.phpro.2011.03.035

[73] Zheng, B., *et al.* (2009) Processing and Behavior of Fe-Based Metallic Glass Components via Laser-Engineered Net Shaping. *Metallurgical and Materials Transactions A*, **40**, 1235-1245. https://doi.org/10.1007/s11661-009-9828-y

[74] Dezfoli, A.R.A., *et al.* (2017) Determination and Controlling of Grain Structure of Metals after Laser Incidence: Theoretical Approach. *Scientific Reports*, **7**, Article ID: 41527. https://doi.org/10.1038/srep41527

[75] Zinoviev, A., *et al.* (2016) Evolution of Grain Structure during Laser Additive Manufacturing. Simulation by a Cellular Automata Method. *Materials & Design*, **106**, 321-329. https://doi.org/10.1016/j.matdes.2016.05.125

[76] Khairallah, S.A., *et al.* (2016) Laser Powder-Bed Fusion Additive Manufacturing: Physics of Complex Melt Flow and Formation Mechanisms of Pores, Spatter, and Denudation Zones. *Acta Materialia*, **108**, 36-45. https://doi.org/10.1016/j.actamat.2016.02.014

[77] Zhang, J., *et al.* (2013) Probabilistic Simulation of Solidification Microstructure Evolution during Laser-Based Metal Deposition. *Proceedings of* 2013 *Annual International Solid Freeform Fabrication Symposium—An Additive Manufacturing Conference*, Austin, TX, 2013.

[78] Lindgren, L.-E., *et al.* (2016) Simulation of Additive Manufacturing Using Coupled

Constitutive and Microstructure Models. *Additive Manufacturing*, **12**, 144-158.

[79] Musaddique Ali Rafique, M. (2018) Simulation of Solidification Parameters during Zr Based Bulk Metallic Glass Matrix Composite's (BMGMCs). *Additive Manufacturing*, **10**, 85-108.

[80] Rafique, M.M.A., Qiu, D. and Easton, M. (2017) Modeling and Simulation of Microstructural Evolution in Zr Based Bulk Metallic Glass Matrix Composites during Solidification. *MRS Advances*, **2**, 3591-3606.

[81] Li, Y. and Gu, D. (2014) Thermal Behavior during Selective Laser Melting of Commercially Pure Titanium Powder: Numerical Simulation and Experimental Study. *Additive Manufacturing*, **1-4**, 99-109. https://doi.org/10.1016/j.addma.2014.09.001

[82] Baufeld, B., Brandl, E. and van der Biest, O. (2011) Wire Based Additive Layer Manufacturing: Comparison of Microstructure and Mechanical Properties of Ti-6Al-4V Components Fabricated by Laser-Beam Deposition and Shaped Metal Deposition. *Journal of Materials Processing Technology*, **211**, 1146-1158. https://doi.org/10.1016/j.jmatprotec.2011.01.018

[83] Li, B., *et al.* (2006) Laser Welding of $Zr_{45}Cu_{48}Al_7$ Bulk Glassy Alloy. *Journal of Alloys and Compounds*, **413**, 118-121.

[84] Pauly, S., *et al.* (2013) Processing Metallic Glasses by Selective Laser Melting. *Materials Today*, **16**, 37-41. https://doi.org/10.1016/j.mattod.2013.01.018

[85] Kim, J.H., *et al.* (2007) Pulsed Nd:YAG Laser Welding of $Cu_{54}Ni_6Zr_{22}Ti_{18}$ Bulk Metallic Glass. *Materials Science and Engineering*: *A*, **449-451**, 872-875. https://doi.org/10.1016/j.msea.2006.02.323

[86] Matthews, D.T.A., Ocelík, V. and de Hosson, J.T.M. (2007) Tribological and Mechanical Properties of High Power Laser Surface-Treated Metallic Glasses. *Materials Science and Engineering*: *A*, **471**, 155-164. https://doi.org/10.1016/j.msea.2007.02.119

[87] Chen, B., *et al.* (2010) Improvement in Mechanical Properties of a Zr-Based Bulk Metallic Glass by Laser Surface Treatment. *Journal of Alloys and Compounds*, **504**, S45-S47. https://doi.org/10.1016/j.jallcom.2010.04.053

[88] Wu, G., *et al.* (2012) Induced Multiple Heterogeneities and Related Plastic Improvement by Laser Surface Treatment in CuZr-Based Bulk Metallic Glass. *Intermetallics*, **24**, 50-55. https://doi.org/10.1016/j.intermet.2012.01.022

[89] Williams, E. and Lavery, N. (2017) Laser Processing of Bulk Metallic Glass: A Review. *Journal of Materials Processing Technology*, **247**, 73-91. https://doi.org/10.1016/j.jmatprotec.2017.03.034

[90] Ouyang, D., Li, N. and Liu, L. (2018) Structural Heterogeneity in 3D Printed Zr-Based Bulk Metallic Glass by Selective Laser Melting. *Journal of Alloys and Compounds*, **740**, 603-609. https://doi.org/10.1016/j.jallcom.2018.01.037

[91] Zhang, C., *et al.* (2018) 3D Printing of Fe-Based Bulk Metallic Glasses and Composites with Large Dimension and Enhanced Toughness by Thermal Spraying. *Journal of Materials Chemistry A*, **6**, 6800-6805.

[92] Ouyang, D., *et al.* (2017) 3D Printing of Crack-Free High Strength Zr-Based Bulk metallic Glass Composite by Selective Laser Melting. *Intermetallics*, **90**, 128-134. https://doi.org/10.1016/j.intermet.2017.07.010

[93] Shen, Y., *et al.* (2017) 3D Printing of Large, Complex Metallic Glass Structures. *Materials & Design*, **117**, 213-222. https://doi.org/10.1016/j.matdes.2016.12.087

[94] Matthews, D.T.A., *et al.* (2009) Laser Engineered Surfaces from Glass Forming Alloy Powder Precursors: Microstructure and Wear. *Surface and Coatings Technolo-*

gy, **203**, 1833-1843. https://doi.org/10.1016/j.surfcoat.2009.01.015

[95] Wang, H.-S., *et al.* (2011) The Effects of Initial Welding Temperature and Welding Parameters on the Crystallization Behaviors of Laser Spot Welded Zr-Based Bulk Metallic Glass. *Materials Chemistry and Physics*, **129**, 547-552. https://doi.org/10.1016/j.matchemphys.2011.04.067

[96] Wang, H.-S., Wu, J.-Y. and Liu, Y.-T. (2016) Effect of the Volume Fraction of the Ex-Situ Reinforced Ta Additions on the Microstructure and Properties of Laser-Welded Zr-Based Bulk Metallic Glass Composites. *Intermetallics*, **68**, 87-94. https://doi.org/10.1016/j.intermet.2015.09.007

[97] Wang, H.S., *et al.* (2010) Combination of a Nd:YAG Laser and a Liquid Cooling Device to $(Zr_{53}Cu_{30}Ni_9Al_8)Si_{0.5}$ Bulk Metallic Glass Welding. *Materials Science and Engineering*: *A*, **528**, 338-341. https://doi.org/10.1016/j.msea.2010.09.014

[98] Zhu, Y., *et al.* (2016) Effect of Nanosecond Pulse Laser Ablation on the Surface Morphology of Zr-Based Metallic Glass. *Optics & Laser Technology*, **83**, 21-27. https://doi.org/10.1016/j.optlastec.2016.03.021

[99] Williams, E. and Brousseau, E.B. (2016) Nanosecond Laser Processing of $Zr_{41.2}Ti_{13.8}Cu_{12.5}Ni_{10}Be_{22.5}$ with Single Pulses. *Journal of Materials Processing Technology*, **232**, 34-42. https://doi.org/10.1016/j.jmatprotec.2016.01.023

[100] Fu, J., *et al.* (2016) Effect of Laser Shock Peening on the Compressive Deformation and Plastic Behavior of Zr-Based Bulk Metallic Glass. *Optics and Lasers in Engineering*, **86**, 53-61. https://doi.org/10.1016/j.optlaseng.2016.05.014

[101] Audebert, F., *et al.* (2003) Production of Glassy Metallic Layers by Laser Surface treatment. *Scripta Materialia*, **48**, 281-286. https://doi.org/10.1016/S1359-6462(02)00382-2

[102] Ma, F., *et al.* (2010) Femtosecond Laser-Induced Concentric Ring Microstructures on Zr-Based Metallic Glass. *Applied Surface Science*, **256**, 3653-3660. https://doi.org/10.1016/j.apsusc.2010.01.003

[103] Heine, R.W., Loper, C.R. and Rosenthal, P.C. (1955) Principles of Metal Casting, McGraw-Hill, New York, NY.

[104] Chalmers, B. (1970) Principles of Solidification, In: Low, W. and Schieber, M., Eds., *Applied Solid State Physics*, Springer, Boston, MA, 161-170. https://doi.org/10.1007/978-1-4684-1854-5_5

[105] Xu, W., *et al.* (2011) *In Situ* Formation of Crystalline Flakes in Mg-Based Metallic Glass Composites by Controlled Inoculation. *Acta Materialia*, **59**, 7776-7786. https://doi.org/10.1016/j.actamat.2011.08.044

[106] Stefanescu, D. (2015) Science and Engineering of Casting Solidification, Springer, Berlin. https://doi.org/10.1007/978-3-319-15693-4

[107] Flemings, M.C. (1974) Solidification Processing. McGraw-Hill, New York, NY.

[108] Christian, J.W. (2002) The Theory of Transformations in Metals and Alloys. Elsevier Science, Amsterdam.

[109] Rafique, M.M.A. (2018) Effect of Inoculation on Phase Formation and Indentation Hardness Behaviour of $Zr_{47.5}Cu_{45.5}Al_5Co_2$ and $Zr_{65}Cu_{15}Al_{10}Ni_{10}$ Bulk Metallic Glass Matrix Composites. Engineering, **10**, 530-559.

[110] Yue, T.M., Su, Y.P. and Yang, H.O. (2007) Laser Cladding of $Zr_{65}Al_{7.5}Ni_{10}Cu_{17.5}$ Amorphous Alloy on Magnesium. *Materials Letters*, **61**, 209-212. https://doi.org/10.1016/j.matlet.2006.04.033

[111] Wang, Y., *et al.* (2004) Microstructure and Properties of Laser Clad Zr-Based Alloy Coatings on Ti Substrates. *Surface and Coatings Technology*, **176**, 284-289.

https://doi.org/10.1016/S0257-8972(03)00771-0

[112] Jiang, S.-S., *et al.* (2018) A CuZr-Based Bulk Metallic Glass Composite with Excellent Mechanical Properties by Optimizing Microstructure. *Journal of Non-Crystalline Solids*, **483**, 94-98. https://doi.org/10.1016/j.jnoncrysol.2018.01.006

[113] Cheng, J.L. and Chen, G. (2013) Glass formation of Zr-Cu-Ni-Al Bulk Metallic Glasses Correlated with L→Zr2Cu+ZrCu Pseudo Binary Eutectic Reaction. *Journal of Alloys and Compounds*, **577**, 451-455. https://doi.org/10.1016/j.jallcom.2013.06.126

[114] Li, P., *et al.* (2014) Glass Forming Ability, Thermodynamics and Mechanical Properties of Novel Ti-Cu-Ni-Zr-Hf Bulk Metallic Glasses. *Materials & Design*, **53**, 145-151. https://doi.org/10.1016/j.matdes.2013.06.060

[115] Ayyagari, A., *et al.* (2018) Electrochemical and Friction Characteristics of Metallic Glass Composites at the Microstructural Length-Scales. *Scientific Reports*, **8**, 906. https://doi.org/10.1038/s41598-018-19488-7

[116] Chen, H.S. (1980) Glassy Metals. *Reports on Progress in Physics*, **43**, 353. https://doi.org/10.1088/0034-4885/43/4/001